Non-linear k–ε–v^2 modeling with application to high-lift

By F. S. Lien[1] AND P. A. Durbin[2]

The $k-\varepsilon-\overline{v^2}$ model has been investigated to quantify its predictive performance on two high-lift configurations: 2D flow over a single-element aerofoil, involving closed-type separation; 3D flow over a prolate spheroid, involving open-type separation. A 'code-friendly' modification has been proposed which enhances the numerical stability, in particular, for explicit and uncoupled flow solvers. As a result of introducing Reynolds-number dependence into a coefficient of the ε-equation, the skin-friction distribution for the by-pass transitional flow over a flat plate is better predicted. In order to improve deficiencies arising from the Boussinesq approximation, a non-linear stress-strain constitutive relation was adopted, in which the only one free constant is calibrated on the basis of DNS data, and the Reynolds-stress anisotropy near the wall is fairly well represented.

1. Introduction

Eddy-viscosity models based on the linear Boussinesq relations are known to be afflicted by numerous weaknesses, including an inability to capture normal stress anisotropy, insufficient sensitivity to secondary strains, seriously excessive generation of turbulence at impingement zones, and a violation of realizability at large rates of strain. Notwithstanding these defects, eddy-viscosity models remain popular, and their use in complex flows is widespread due, principally, to their formalistic simplicity, numerical robustness, and computational economy. Second-moment closure, on the other hand, accounts for several of the key features of turbulence that are misrepresented by linear eddy-viscosity models, but is considerably more complex and can suffer from poor numerical stability due to the lack of dominance of second-order fragments in the set of terms representing diffusion. As a result, the CPU requirements for second-moment closure models can be high, especially in 3D flows.

A potential alternative to second-moment closure, but one which retains advantageous elements of the linear eddy-viscosity framework, is to use a constitutive relation that equates the Reynolds-stresses to a non-linear expansion in powers of the mean rate of strain and rate of rotation tensors. This may be cast in the form of a sum of terms, each pre-multiplied by an apparent viscosity—hence the term 'non-linear eddy-viscosity models'. Examples include the models of Speziale (1987), Shih *et al.* (1993), Durbin (1995a), Craft *et al.* (1995) and Lien *et al.* (1996). The

1 University of Manchester Institute of Science and Technology, UK
2 Stanford University

main differences between the above modeling strategies can be summarized in the following table:

Authors(s)	Model form	Order in the stress-strain relationship	Number of turbulence transport equations
Speziale (1987)	High-Re	quadratic	2, $k-\varepsilon$
Shih *et al.* (1993)	High-Re	quadratic	2, $k-\varepsilon$
Durbin (1995a)	Low-Re	quadratic	3, $k-\varepsilon-\overline{v^2}$
Craft *et al.* (1995)	Low-Re	cubic	3, $k-\varepsilon-A_2$
Lien *et al.* (1996)	Low-Re	cubic	2, $k-\varepsilon$

The A_2 value—the second Reynolds-stress invariant—in Craft *et al.*'s $k-\varepsilon-A_2$ model is obtained by solving a related transport equation as follows:

$$\partial_t A_2 + U\cdot\nabla A_2 = -2\frac{A_2}{k}(d_k + P_k - \varepsilon)$$
$$+2\frac{a_{ij}}{k}(d_{ij} + P_{ij} + \phi_{ij} - \varepsilon_{ij}), \tag{1}$$

with fragments consistent with second-moment closure. In order to be free from topological constraints, the unit vector in the wall-reflection term is replaced by the length-scale gradient. The expansion of (1) in 3D curvilinear coordinate systems is tedious and prone to error. Also, a major drawback of this model is the high level of sensitivity to the near-wall grid parameters, including resolution, distribution, and aspect ratio.

The $\overline{v^2}$-equation in Durbin's $k-\varepsilon-\overline{v^2}$ model, to be addressed in Section 2, was simplified from second-moment closure on the basis of the IP pressure-strain model in conjunction with elliptic relaxation. This approach is algorithmically simple, applicable to the low-Re region, and naturally mimics the kinematic blocking effect on the turbulence of a solid wall.

Another important feature which distinguishes Durbin's model from most others is the expression of eddy-viscosity ν_t, which plays an important role in determining the correct level of shear stress. In Craft *et al.*'s model,

$$\nu_t = 0.734\frac{r_\eta[1-\exp\{-0.145\exp(1.3\eta^{5/6})\}]}{1+1.8\eta}\frac{\sqrt{\tilde{\epsilon}/\epsilon}\{1-0.8\exp(-\tilde{R}_t/30)\}}{1+0.6A_2+0.2A_2^{3.5}}\,(kT) \tag{2}$$

where

$$r_\eta = 1+\left[1-\exp(-\frac{A_2^3}{0.125})\right]\left[1+4\sqrt{\exp(-\tilde{R}_t/20)}\right],\ \eta = \max(\tilde{S},\tilde{\Omega})r_\eta, \tag{3}$$

and $\tilde{S}$ and $\tilde{\Omega}$ are strain and vorticity invariants. While in Durbin's model,

$$\nu_t = 0.19\frac{\overline{v^2}}{k}(kT). \tag{4}$$

One distinct difference between Eqs. (2) and (4) is that the latter does not require any damping function: a result of using $\overline{v^2}$ as the velocity scale in the direction of the wall. The former, on the other hand, sensitizes ν_t to $\tilde{S}$, $\tilde{\Omega}$, $\tilde{R}_t$ (i.e., Reynolds number) and A_2, with the functional dependency being carefully calibrated on a range of flows, including straining flow, channel flow, impinging jet, and transitional flow. However when this model was tested for turbomachinery flows at (and near) off-design conditions, the size of the leading-edge separation bubble was overestimated, and in some cases no converged solution could be obtained. This is due to η (strain and vorticity) and A_2 being too large along the curved shear layer . As a result of both parameters appearing in the denominator of ν_t expression, the level of shear stress was significantly under-predicted (Chen, 1996).

In the present work, the $k-\varepsilon-\overline{v^2}$ model of Durbin (1995b) is applied to high-lift configurations, both 2D and 3D. In the course of this study, numerical instability arising from the boundary condition at wall was encountered, due to our use of a solution algorithm that uncouples the $\overline{v^2}$ and f-equations. A 'code-friendly' modification is introduced, which not only circumvents this numerical difficulty, but also gives better predictions for transitional flows. This variant is then combined with the non-linear stress-strain constitutive equation with the aim of improving the near-wall behavior of normal-stress anisotropy.

2. $k-\varepsilon-\overline{v^2}$ model

The turbulence model uses the standard $k-\varepsilon$ equations:

$$\partial_t k + U\cdot\nabla k = P_k - \varepsilon + [(\nu + \frac{\nu_t}{\sigma_k})\nabla k], \tag{5}$$

$$\partial_t \varepsilon + U\cdot\nabla \varepsilon = \frac{C_{\epsilon 1}P_k - C_{\epsilon 2}\varepsilon}{T} + [(\nu + \frac{\nu_t}{\sigma_\epsilon})\nabla \varepsilon]. \tag{6}$$

On no-slip boundaries, $y \to 0$,

$$k = 0,\ \epsilon \to 2\nu\frac{k}{y^2}. \tag{7}$$

The $\overline{v^2}$ transport equation is

$$\partial_t \overline{v^2} + U\cdot\nabla \overline{v^2} = kf - n\overline{v^2}\frac{\varepsilon}{k} + \nabla\cdot[(\nu+\nu_t)\nabla\overline{v^2}], \tag{8}$$

where kf represents redistribution of turbulence energy from the streamwise component. Non-locality is represented by solving an elliptic relaxation equation for f:

$$L^2\nabla^2 f - f = \frac{1}{T}\left[(C_1 - n)\frac{\overline{v^2}}{k} - (C_1 - 1) - \frac{2}{3}\right] - C_2\frac{P_k}{k}, \tag{9}$$

where

$$T = \max\left[\frac{k}{\varepsilon}, 6(\frac{\nu}{\varepsilon})^{1/2}\right],\ L = C_L\max\left[\frac{k^{3/2}}{\varepsilon}, C_\eta(\frac{\nu^3}{\varepsilon})^{1/4}\right]. \tag{10}$$

The Boussinesq approximation is used for the stress-strain relation:

$$a_{ij} = \frac{\overline{u_i u_j}}{k} - \frac{2}{3}\delta_{ij} = -\frac{\nu_t}{k} S_{ij}, \tag{11}$$

where the eddy viscosity is given by

$$\nu_t = C_\mu \overline{v^2} T. \tag{12}$$

The constants of the model are:

$$C_\mu = 0.19,\ \sigma_k = 1,\ \sigma_\epsilon = 1.3,$$

$$C_{\epsilon 1} = 1.55,\ C_{\epsilon 2} = 1.9$$

$$C_1 = 1.4,\ C_2 = 0.3,\ C_L = 0.3,\ C_\eta = 70. \tag{13}$$

As $y \to 0$ — y being the minimum distance to walls — and $k \to (1/2\nu)\varepsilon y^2$, Eq. (8) becomes:

$$\nu \partial_y^2 \overline{v^2} - 2n\nu \frac{\overline{v^2}}{y^2} = kf. \tag{14}$$

The viscous and kinematic conditions at the wall show that $\overline{v^2}$ should be $O(y^4)$ as $y \to 0$. In the original $k - \varepsilon - \overline{v^2}$ model, $n = 1$, yielding the boundary condition for f

$$f(0) \to -\frac{(24 - 4n)\nu^2 \overline{v^2}}{\varepsilon(0) y^4}\Big|_{n=1} = -\frac{20\nu^2 \overline{v^2}}{\varepsilon(0) y^4}. \tag{15}$$

on no-slip walls.

2.1 Code-friendly modification

Equation (15) works fairly well for coupled, implicit solvers [e.g. INS2D code of Rogers & Kwak (1990)]. However, for explicit and uncoupled schemes, numerical instability arising from y^4 in the denominator of Eq. (15) sometimes occurs. Therefore, a code-friendly modification is made here by setting $n = 6$, which allows $f(0) = 0$ to be imposed as the boundary condition. In addition, $C_{\epsilon 1}$ and $C_{\epsilon 2}$ are replaced by

$$C_{\epsilon 1} = 1.55 + \exp(-A_\epsilon R_y^2)|_{A_\epsilon = 0.00285},\ C_{\epsilon 2} = 1.92, \tag{16}$$

where $R_y = y\sqrt{k}/\nu$, and the other model constants are:

$$C_\mu = 0.19,\ \sigma_k = 1,\ \sigma_\epsilon = 1.5,$$

$$C_1 = 1.4,\ C_2 = 0.3,\ C_L = 0.17\ C_\eta = 70. \tag{17}$$

2.1.1 Fully-developed channel flow

The model constants, in particular $A_\epsilon = 0.00285$ and $C_L = 0.17$, were first calibrated with the channel-flow DNS data of Kim *et al.* (1987) and then optimized

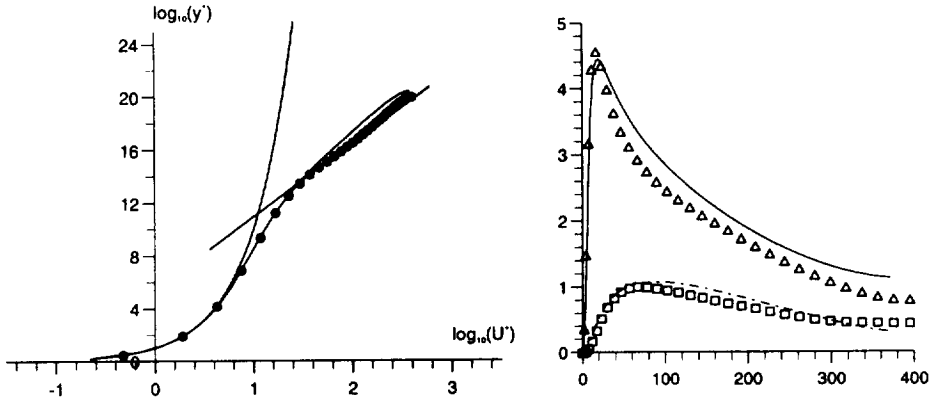

FIGURE 1. Channel flow: (Left) mean velocity; (Right) k and $\overline{v^2}$. DNS: • velocity; △ k; □ $\overline{v^2}$.

on the basis of 2D/3D separated flows to be presented later. As seen in Fig. 1, both the mean-velocity and turbulence profiles, the latter including k and $\overline{v^2}$, agree reasonably well with the data.

2.1.2 By-pass transitional flow over a flat plate

The second case examined here is the flow over a flat plate with free-stream turbulence intensity $T_u = 3\%$ and dissipation length scale $\ell_\varepsilon^\infty = 10$ mm. The experimental study was conducted at Rolls Royce Aeroengines in Derby, UK. The skin-friction distributions, obtained with the original and code-friendly $k-\varepsilon-\overline{v^2}$ variants and Launder-Sharma model (1974), are shown in Fig. 2(L). As seen, introducing the R_y-dependency in $C_{\epsilon 1}$ for the code-friendly variant improves transition predictions. Although the resulting onset of transition is slightly earlier than that returned by the Launder-Sharma model, the length of transition is better represented. As the flow becomes fully turbulent, the velocity profiles obtained with both $k-\varepsilon-\overline{v^2}$ variants are almost identical as demonstrated in Fig. 2(R).

2.2 Non-linear constitutive relation

A general constitutive relation of the type proposed by Pope (1975) can be written as:

$$a_{ij} = \frac{\overline{u_i u_j}}{k} - \frac{2}{3}\delta_{ij} = \sum_{\lambda=1}^{10} G^\lambda(S_{ij}, \Omega_{ij}, \overline{v^2}/k, T) T_{ij}^\lambda. \tag{18}$$

where $T_{ij}^1 = S_{ij}$, $T_{ij}^2 = S_{ik}\Omega_{kj} - \Omega_{ik}S_{kj}$, $T_{ij}^3 = S_{ik}S_{kj} - \frac{1}{3}\delta_{ij}S_{lk}S_{kl}\cdots$. Truncating at the third term for simplicity gives rise to

$$a_{ij} = -\frac{\nu_t}{k}S_{ij} + G^2(S_{ik}\Omega_{kj} - \Omega_{ik}S_{kj}) + G^3(S_{ik}S_{kj} - \frac{1}{3}\delta_{ij}S_{lk}S_{kl}). \tag{19}$$

where

$$S_{ij} = \frac{\partial U_i}{\partial x_j} + \frac{\partial U_j}{\partial x_i}, \quad \Omega_{ij} = \frac{\partial U_i}{\partial x_j} - \frac{\partial U_j}{\partial x_i}. \tag{20}$$

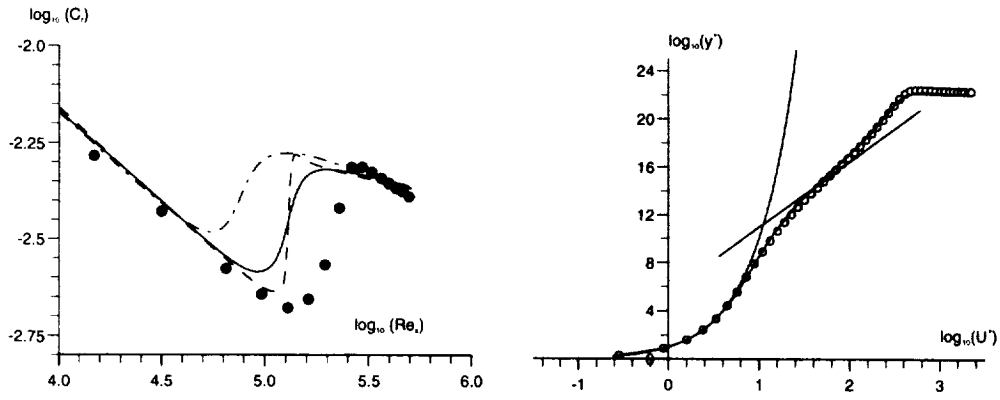

FIGURE 2. Flat plate: (Left) skin friction; (Right) mean-velocity profile. • expt.; ---- $k-\varepsilon$; —·— o original $k-\varepsilon-\overline{v^2}$; —— modified $k-\varepsilon-\overline{v^2}$

Two constrains for parallel flow will be imposed:

$$a_{22} = a_{\overline{v^2}}, \quad a_{11} = \alpha a_{22} = \alpha a_{\overline{v^2}}, \tag{21}$$

where $a_{\overline{v^2}} = \frac{\overline{v^2}}{k} - \frac{2}{3}$. These yield

$$G^2 = \frac{1}{4}\frac{(1-\alpha)a_{\overline{v^2}}}{S^2}T^2, \quad G^3 = \frac{3}{2}\frac{(1+\alpha)a_{\overline{v^2}}}{S^2}T^2, \tag{22}$$

where $S = \frac{k}{\varepsilon}|\frac{\partial U}{\partial y}|$ or $(= \frac{k}{\varepsilon}\sqrt{S_{ij}S_{ij}/2}$, in general) and T is defined in Eq. (6). The remaining unknown, α, can be evaluated from DNS data of channel flow (Kim *et al.*, 1987), boundary-layer flow (Spalart, 1988) and flow over a backward-facing step (Le *et al.*, 1993). As seen in Fig. 3,

$$\alpha = -1 - \frac{6S}{15+10S} \tag{23}$$

fits DNS data reasonably well. The algebraic model was initially used by Durbin (1995a) as an *a postiori* formula for evaluating $\overline{u_iu_j}$. In order to apply Eq. (19) to mean flow prediction while preventing computational intractability, the coefficients G^2 and G^3 are modified as:

$$G^2 = \frac{1}{4}\frac{(1-\alpha)a_{\overline{v^2}}}{S^2+1}T^2, \quad G^3 = \frac{3}{2}\frac{(1+\alpha)a_{\overline{v^2}}}{S^2+1}T^2. \tag{24}$$

3. Numerical method

All flows have been computed with the STREAM general geometry, block-structured, finite-volume code (Lien & Leschziner, 1994a). Advection is approximated by a TVD scheme with the UMIST limiter (Lien & Leschziner, 1994b). To avoid checkerboard oscillations within the co-located storage arrangement, the "Rhih and Chow" interpolation method (1983) is used. The solution is effected by an iterative pressure-correction SIMPLE algorithm, applicable to both subsonic and transonic conditions (Lien & Leschziner, 1993).

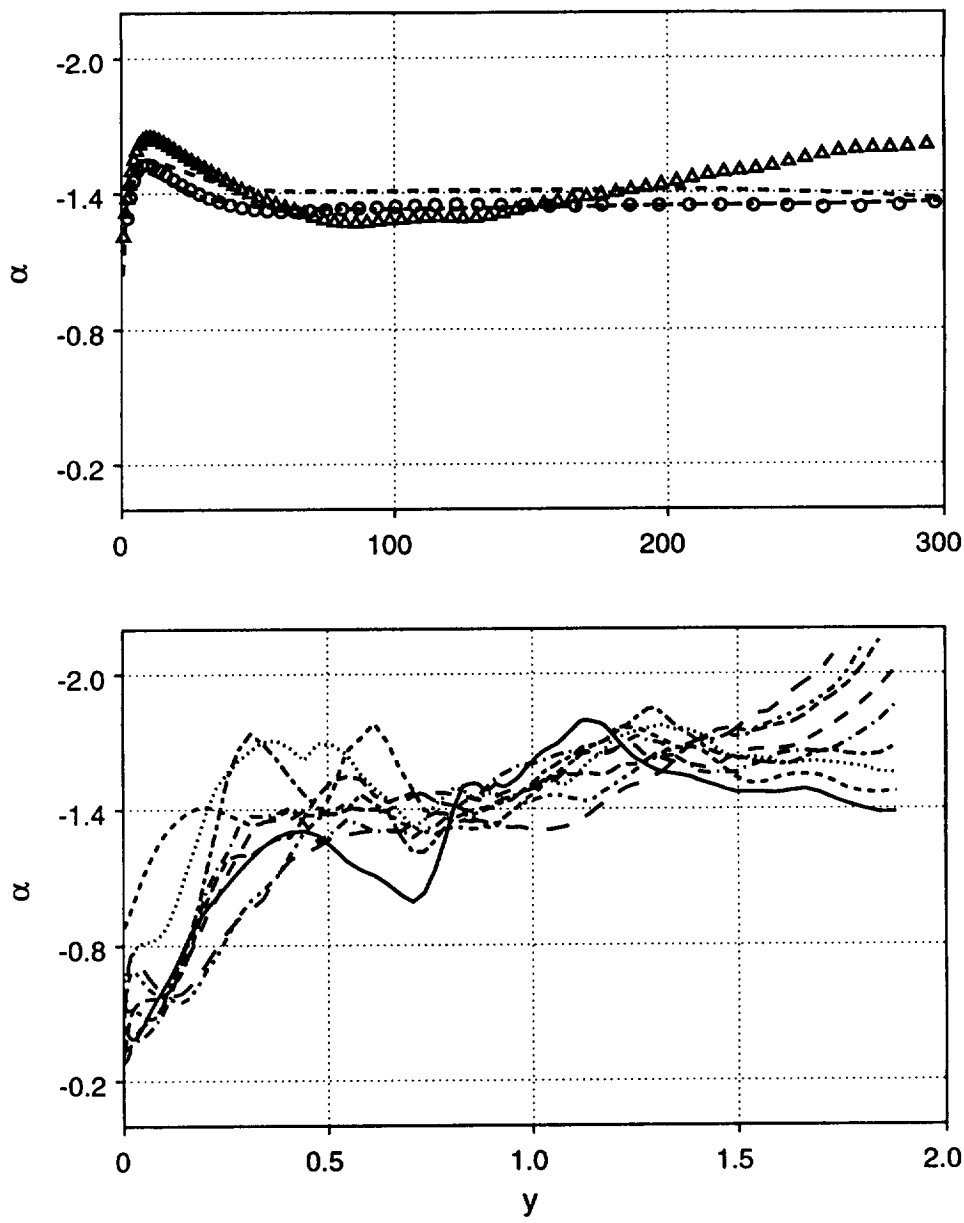

FIGURE 3. Correlation of α in the non-linear constitutive equation with DNS data. Top: DNS channel: $R_\tau = 395$, $\triangle$; formula, ---- . DNS boundary layer: $R_\theta = 1410$ o ; formula, —— . Bottom: Backstep DNS: $x = 1$, ——— ; $x = 2$, ---- ; $x = 3$, ····· ; $x = 4$, —— ; $x = 5$, —·— ; $x = 6$, —— ; $x = 7$, —·— - ; $x = 8$, —··— ; $x = 9$, — —.

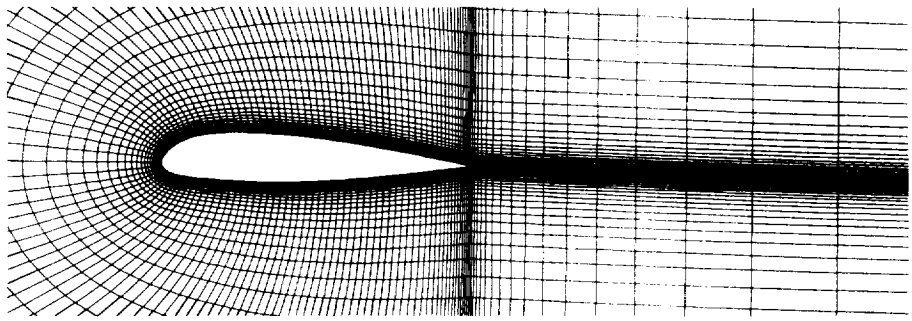

FIGURE 4. A-aerofoil: geometry and partial grid

4. Results and discussion

4.1 Aerospatiale A-aerofoil

Computations for the A-aerofoil have been performed at 13.3° incidence, with transition on the suction side prescribed at 12% of chord. The geometry and a partial view of the grid are given in Fig. 4. The Reynolds number, based on free-stream velocity and chord length, is 2.1×10^6. Solutions have been obtained on a grid containing 177×65 lines, extending to 10 chords into the free stream.

In total, four turbulence-model variants have been applied to this case [comparisons to second-moment closure can be found in Lien & Leschziner (1995)]:

(1) the low-Re $k-\varepsilon$ model of Lien & Leschziner (1993);
(2) the original $k-\varepsilon-\overline{v^2}$ model of Durbin (1995b);
(3) the code-friendly variant;
(4) the above variant combined with the non-linear stress-strain relation.

The skin-friction and wall-pressure distributions obtained with three linear eddy-viscosity models, one $k-\varepsilon$ and two $k-\varepsilon-\overline{v^2}$, are compared in Fig. 5. These, as well as the associated profiles of streamwise velocity and shear stress on the suction side in Figs. 6-7, clearly demonstrate the superiority of $k-\varepsilon-\overline{v^2}$ variants relative to the conventional $k-\varepsilon$ model.

Attention is turned next to comparisons between linear and non-linear $k-\varepsilon-\overline{v^2}$ models in Figs. 8–10 for profiles of streamwise velocity and Reynolds normal-stresses. It is found from these figures that the Reynolds-stress anisotropy is fairly well predicted by the non-linear model at x/c=0.5, which is consistent with the constraints in Eq. (21) imposed on the constitutive equation. As the flow approaches the trailing edge, streamline curvature arising from secondary strain becomes important and the omission of its production term ($\sim \frac{\partial v}{\partial x}$) in the $\overline{v^2}$-equation is no longer valid, resulting in large discrepancies between predictions and data at x/c=0.9.

4.2 DLR prolate spheroid

The shape of this body and a partial view of the numerical grid surrounding it are shown in Fig. 11. The Reynolds number, based on the chord, is 6.5×10^6.

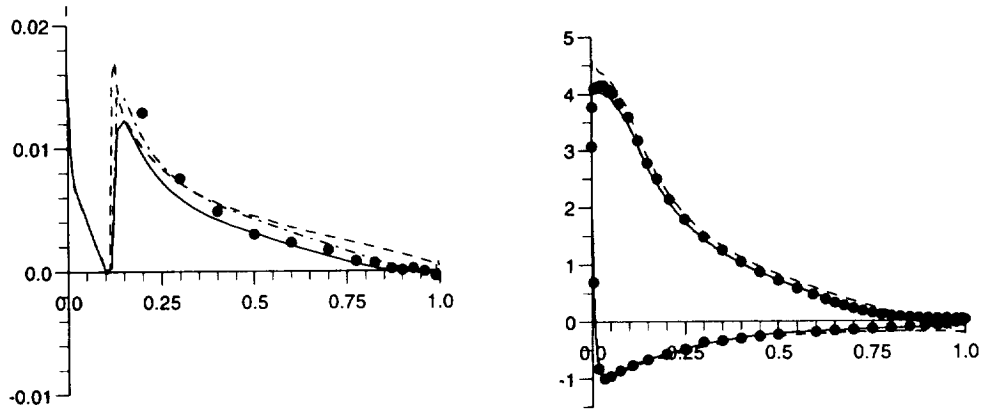

FIGURE 5. A-aerofoil: (Left) skin friction; (Right) pressure coefficient. • expt.; ---- $k-\varepsilon$; —— original $k-\varepsilon-\overline{v^2}$; —·— modified $k-\varepsilon-\overline{v^2}$

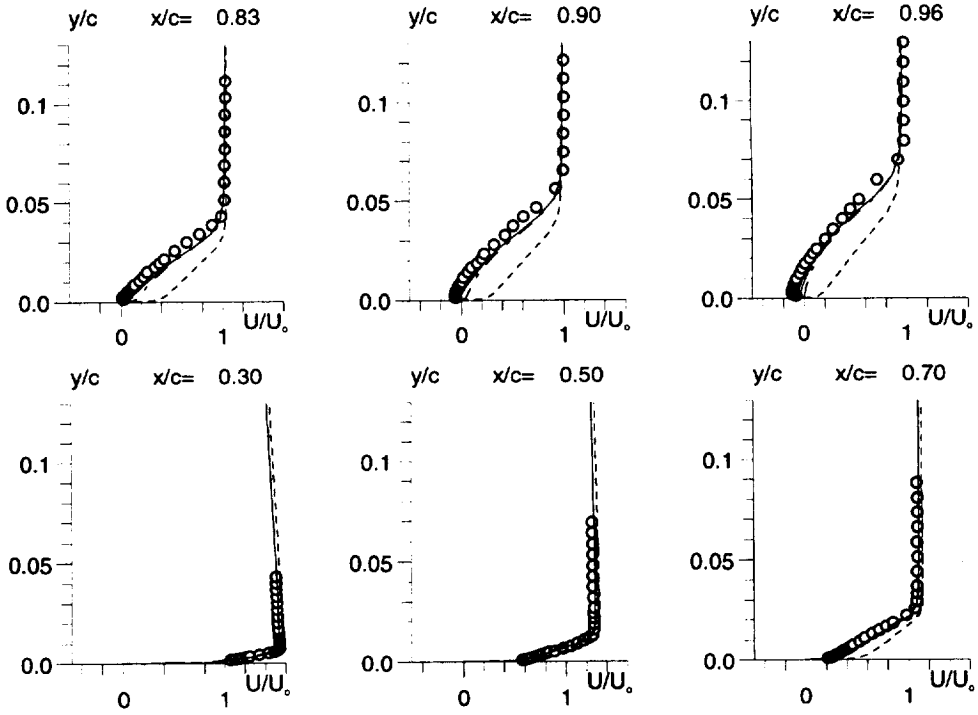

FIGURE 6. A-aerofoil: profiles of streamwise velocity. o expt.; ---- $k-\varepsilon$; —— original $k-\varepsilon-\overline{v^2}$; —·— modified $k-\varepsilon-\overline{v^2}$

Computations have been performed at 30° incidence in which transition is free. The solution domain, containing $65\times65\times65$ lines, extends 10 chords into the outer

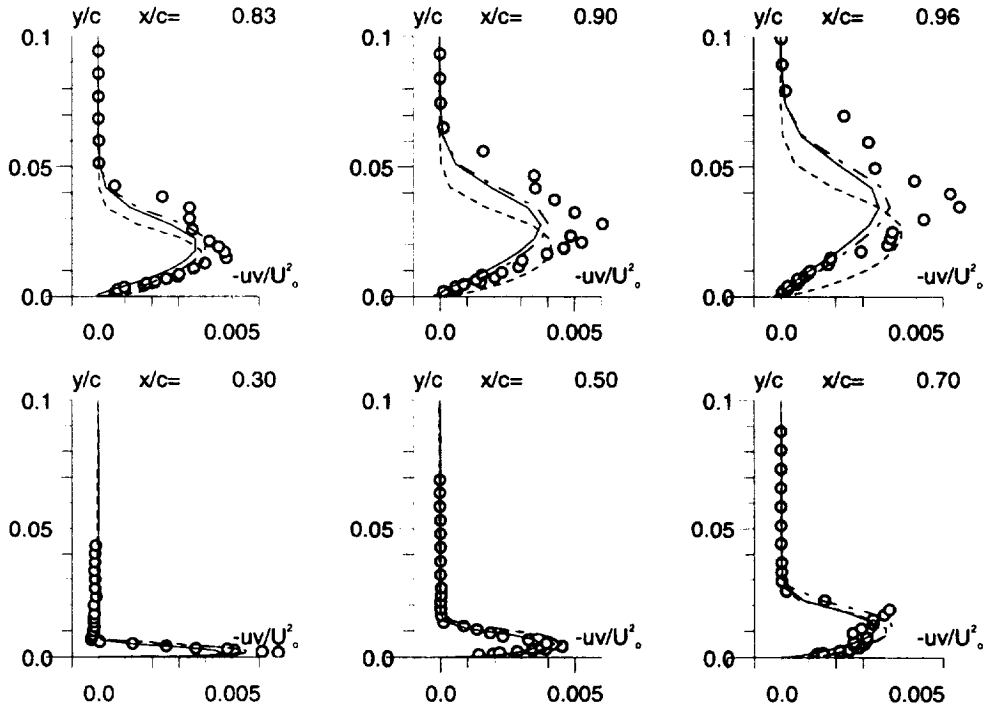

FIGURE 7. A-aerofoil: profiles of shear stress. o expt.; ---- $k-\varepsilon$; ——— original $k-\varepsilon-\overline{v^2}$; —·— modified $k-\varepsilon-\overline{v^2}$

stream.

Numerical solutions have been obtained with two models [comparisons with second-moment closure can be found in Lien & Leschziner (1995b)]:

(1) the low-Re $k-\epsilon$ model of Lien & Leschziner (1993);

(2) the code-friendly $k-\varepsilon-\overline{v^2}$ variant in conjunction with Launder and Kato's modification in the turbulence production P_k (1993).

A well-known defect of any conventional, linear eddy-viscosity model is that it predicts excessive levels of turbulence energy in impingement regions, due to the fact that the irrotational strains appearing in the turbulence-energy equation ($\sim S_{ij}S_{ij}$) act to generate turbulence irrespective of their sign. The rationale behind Launder & Kato's proposal is to partially replace the strain by the vorticity, i.e.

$$P_k = 0.5\nu_t S_{ij}\Omega_{ij}. \tag{25}$$

A similar idea, based on 'realizability' constraints on the turbulence time scale, has been suggested recently by Durbin (1996), in which a upper bound to k/ε proportion to $\sqrt{2/S_{ij}S_{ij}}$ was introduced. As a result, the rate of turbulence-energy generation in the vicinity of stagnation regions becomes *linear*, which is similar to that returned by most of the non-linear eddy-viscosity models mentioned in Section

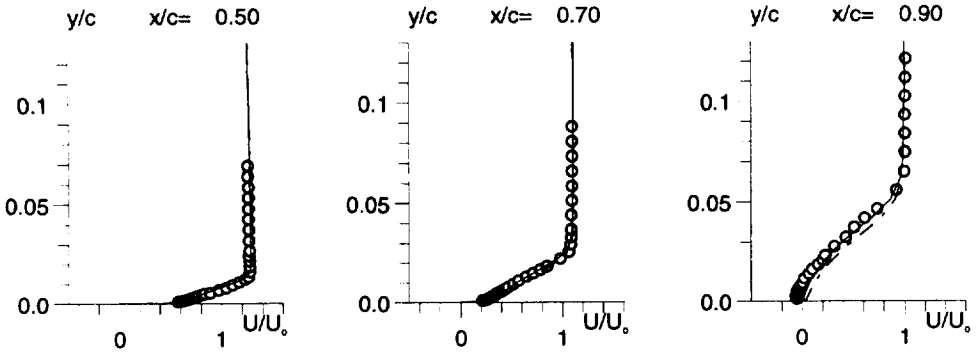

FIGURE 8. A-aerofoil: profiles of streamwise velocity. o expt.; — - — linear $k-\varepsilon-\overline{v^2}$; ——— non-linear $k-\varepsilon-\overline{v^2}$

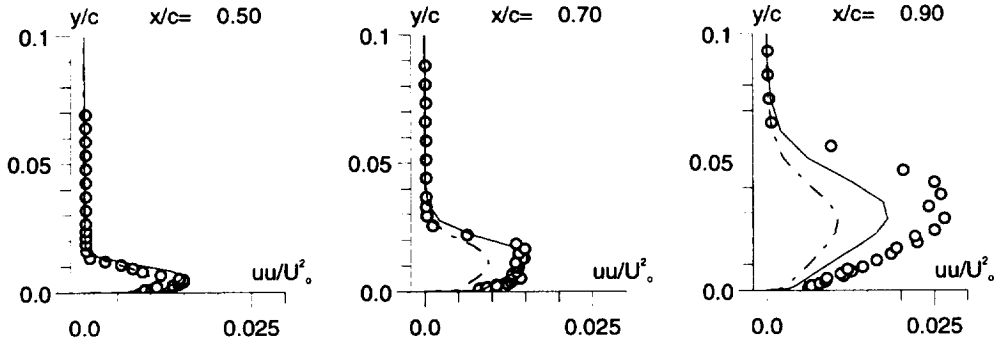

FIGURE 9. A-aerofoil: profiles of streamwise normal stress. o expt.; — - — linear $k-\varepsilon-\overline{v^2}$; ——— non-linear $k-\varepsilon-\overline{v^2}$

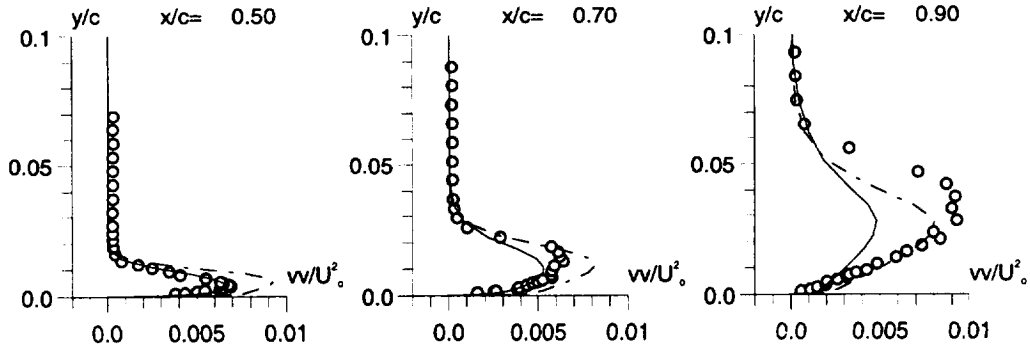

FIGURE 10. A-aerofoil: profiles of transverse normal stress. o expt.; — - — linear $k-\varepsilon-\overline{v^2}$; ——— non-linear $k-\varepsilon-\overline{v^2}$

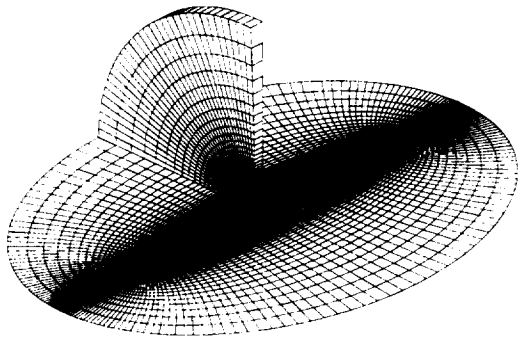

FIGURE 11. Prolate spheroid: geometry and partial grid

1; those models use

$$C_\mu \sim \frac{\alpha}{1 + \beta\sqrt{0.5 S_{ij} S_{ij}}}. \tag{26}$$

Azimuthal variations of skin-friction magnitude and direction at four streamwise locations are shown in Figs. 12 and 13, and the circumferential distributions of wall pressure are given in Fig. 14. As seen at $x/2a = 0.223$, the $k - \varepsilon - \overline{v^2}$ model in conjunction with Launder & Kato's modification returns a transition-like behavior in the boundary layer close to the windward side. Although the model is unable on fundamental grounds to predict any aspect of *natural* transition, the predicted transitional phenomenon is mainly due to a strong suppression of turbulence energy at the impingement regions, in which the flow becomes 'laminar', combined with the fact that the free-stream turbulence diffuses into the boundary layer and ultimately triggers transition. It is clear from Fig. 14 that the extent of pressure plateau regions, signifying the azimuthal extent of separation zone, at $x/2a > 0.564$ are under-estimated by both models. This observation is consistent with the azimuthal distributions of skin-friction direction γ shown in Fig. 13; $\gamma = 0$ denotes either the separation or the reattachment point. The performance of $k - \varepsilon - \overline{v^2}$ model is slightly better than that of $k - \varepsilon$ in terms of the extent of the separation zone. Some of the discrepancies between predictions and experiment might be due to the grid density adopted here; in particular, close to the rear end of the spheroid it is too coarse and a grid-refinement test is required.

5. Conclusions

A computational study has been undertaken to investigate the predictive capabilities of $k - \varepsilon - \overline{v^2}$ variants when applied to high-lift configurations, including 2D aerofoil and 3D prolate spheroid. Both the linear and non-linear stress-strain constitutive relations are examined. The outcome of the present study may be summarized as follows:

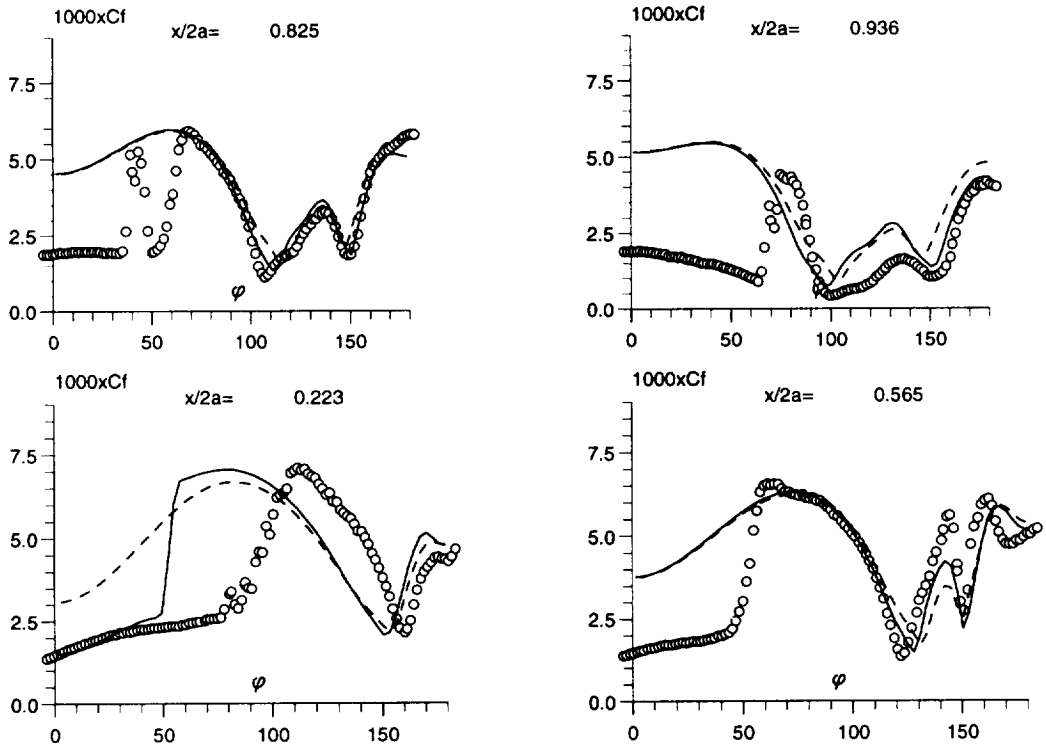

FIGURE 12. Prolate spheroid: skin-friction magnitude. o expt.; ---- $k-\epsilon$; —— modified $k-\epsilon-\overline{v^2}$;

(1) The $k-\varepsilon-\overline{v^2}$ model and its variants, whether linear or non-linear, return superior predictions relative to the conventional $k-\varepsilon$ model.

(2) This superiority can be attributed to the use of $\overline{v^2}$ as the velocity scale in the eddy-viscosity expression without resorting to an *ad hoc* damping function.

(3) The $\overline{v^2}$ is obtained from a simplified form of Reynolds-stress transport equation, governing the turbulence intensity normal to streamlines, the pressure-strain term of which is represented mathematically by an elliptic relaxation model.

(4) A code-friendly modification is proposed here, including the assurance of the near-wall behavior $\overline{v^2} \to O(y^4)$ as $y \to 0$, the introduction of R_y-dependency in $C_{\epsilon 1}$, and the use of $f = 0$ as the boundary condition on no-slip boundaries. As a result, the numerical stability, in particular, for the uncoupled solution procedure used herein is greatly enhanced.

(5) The introduction of R_y in $C_{\epsilon 1}$ yields improved results for the transitional flow. However, it requires the minimum distance to walls, which can be difficult to apply to complex geometries.

(6) Following a similar idea suggested by Durbin & Laurence (1996), a first attempt

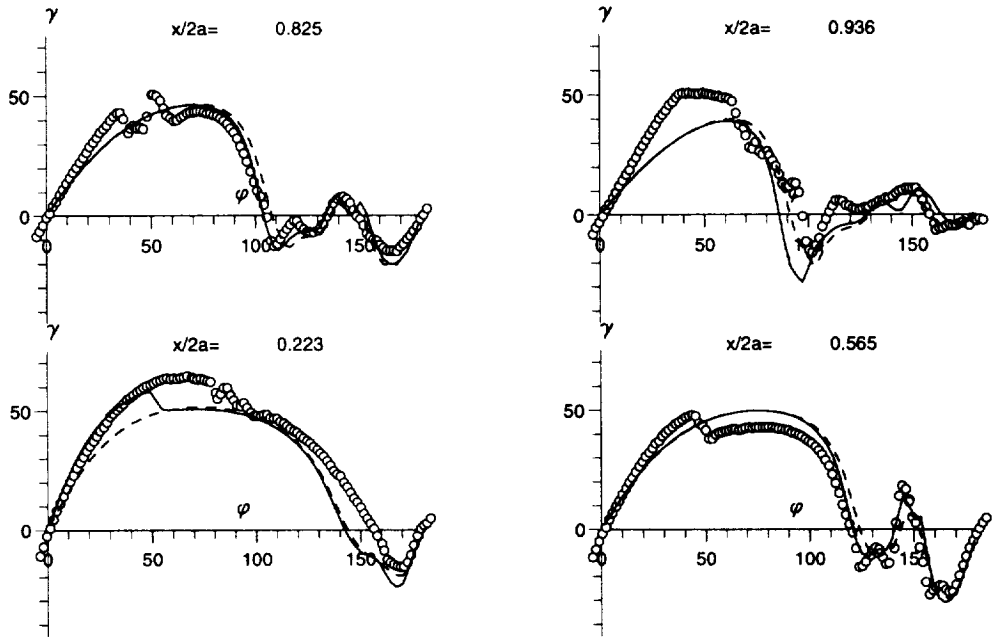

FIGURE 13. Prolate spheroid: skin-friction direction. o expt.; ---- $k-\epsilon$; —— modified $k-\epsilon-\overline{v^2}$;

has been made by adopting

$$C_{\epsilon 1} = 1.44(1 + 0.0333\sqrt{k/\overline{v^2}}),\ C_{\epsilon 2} = 1.85,\ C_L = 0.188,$$

and preliminary results for flows over a flat plate and the A-aerofoil, described in Sections 2.1.1-2.1.2, are given in Figs. 15-17. As seen, the use of $\sqrt{k/\overline{v^2}}$ returns very similar mean-velocity profiles for the A-aerofoil case. However, the onset of transition for the flat-plate case is too early and the length of transition is too long.

(7) In order to improve the performance of $k-\varepsilon-\overline{v^2}$ model for both transitional and fully turbulent flows, in particular, in complex geometries, instead of adopting R_y and $\sqrt{k/\overline{v^2}}$, there is a need to devise a new parameter, depending on the local Reynolds number and avoiding the use of the minimum distance to walls.

(8) The level of normal stress anisotropy returned by the non-linear model is fairly well represented at the mid-chord of A-aerofoil, where the curvature effect is unimportant. Close to the trailing edge, however, both $\overline{u^2}$, $\overline{v^2}$ and, consequently, k and its production P_k are under-predicted. Since $P_k = \nu_t(\frac{\partial U_i}{\partial x_j} + \frac{\partial U_j}{\partial x_i})\frac{\partial U_i}{\partial x_j} + \cdots$ and the mean-velocity profile and, hence, its gradient at $x/c = 0.9$ are in good agreement with the data, this indicates that ν_t is too low, which is consistent with the under-estimation of $\overline{v^2}$ at the same location.

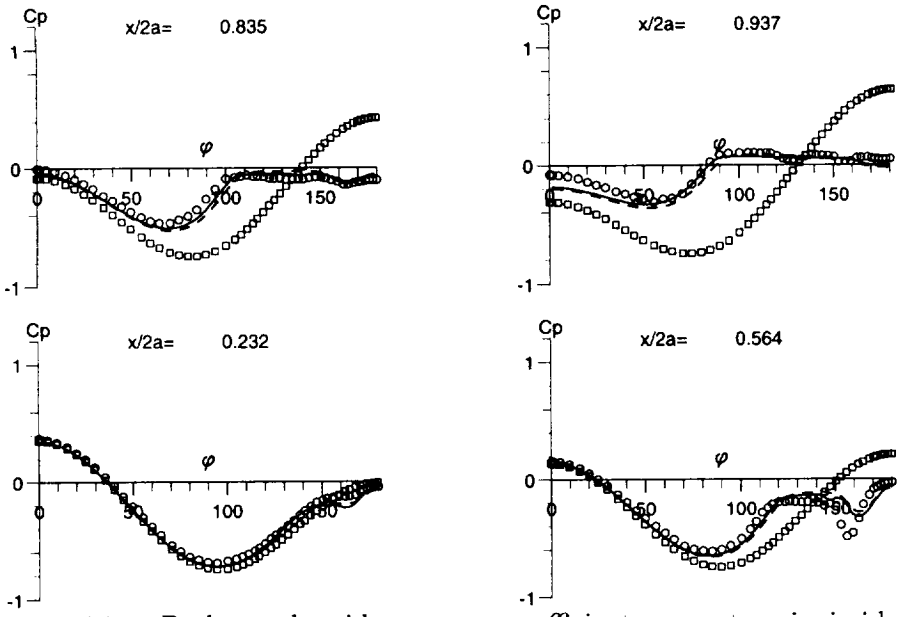

FIGURE 14. Prolate spheroid: pressure coefficient. ○ expt.; □ inviscid solution; ---- $k-\epsilon$; —— modified $k-\epsilon-\overline{v^2}$;

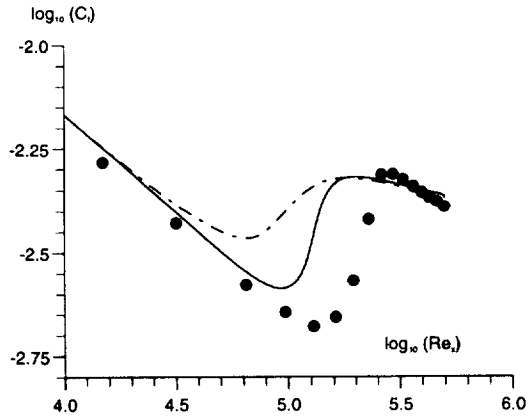

FIGURE 15. Flat plate: skin friction. • expt.; —— based on R_y; — — — based on $\sqrt{k/\overline{v^2}}$

(9) For open 3D separation, the size of separation zone, reflected by the azimuthal extent of pressure plateau, is slightly under-predicted by the $k-\varepsilon-\overline{v^2}$ model, which might be partially attributed to the grid density adopted here being insufficient.

(10) To ensure a wide range of applicability of the non-linear model, the free coefficients

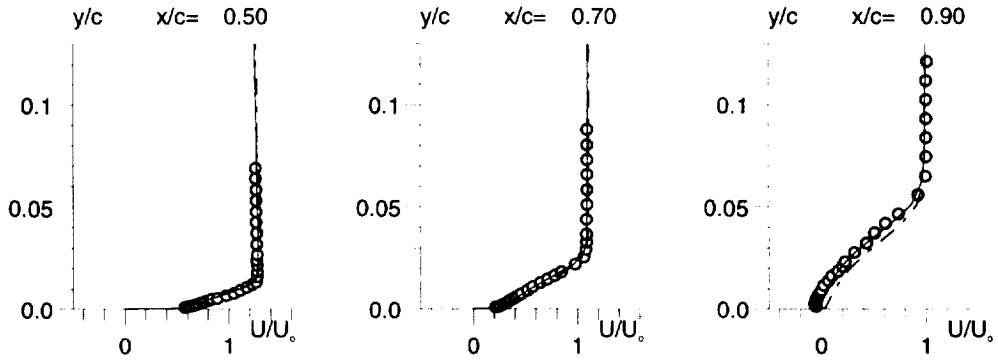

FIGURE 16. A-aerofoil: profiles of streamwise velocity. o expt.; —— based on R_y; — — — based on $\sqrt{k/\overline{v^2}}$

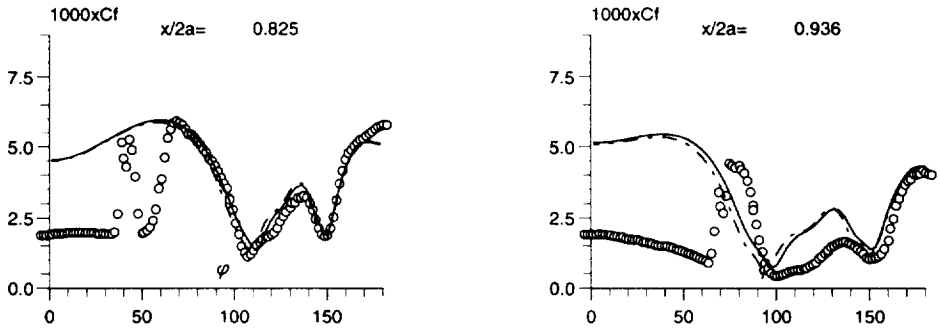

FIGURE 17. Prolate spheroid: skin-friction magnitude. o expt.; —— based on R_y; —·— based on $\sqrt{k/\overline{v^2}}$

and their associated functionals need to be more carefully optimized by reference to different types of flow, featuring separation, impingement, swirl, rotation, and transition.

Acknowledgments

The first author would like to express his gratitude to CTR, UMIST and the Royal Academy of Engineering in the UK for their financial support.

REFERENCES

CHEN, W. L. 1996 *Turbulence Modeling for highly-loaded cascade blade.* Ph.D Thesis, University of Manchester Institute of Science and Technology, UK.

CRAFT, T. J., LAUNDER, B. E. & SUGA, K. 1995 A non-linear eddy viscosity model including sensitivity to stress anisotropy. *Proc. 10th Symp. on Turbulent Shear Flows.* **2,** 23.19-23.24.

DURBIN, P. A. 1995a Constitutive equation for the $k-\varepsilon-\overline{v^2}$ model. *Proc. 6th Int. Symp. on Computational Fluid Dynamics.* **1,** 258-262.

DURBIN, P. A. 1995b Separated flow computations with the $k-\varepsilon-\overline{v^2}$ model. *AIAA J.* **33,** 659-664.

DURBIN, P. A. 1996 On the $k-\epsilon$ stagnation point anomaly. *Int. J. Heat and Fluid Flow.* **17,** 89-90.

DURBIN, P. A. & LAURENCE, D. 1996 Non-local effects in single point closure. *Advances in Turbulence Research,* Seoul, Korea, May 17, 1996, 109-120.

LAUNDER, B. E. & SHARMA, B. I. 1974 Application of energy-dissipation model of turbulence to the calculation of flow near a spinning disc. *Letters in Heat and Mass Transfer.* **1,** 131-138.

LAUNDER, B. E. & KATO, M. 1993 Modeling flow-induced oscillations in turbulent flow around a square cylinder. *ASME FED.* **157,** 189-199.

LE, H., MOIN, P. & KIM, J. 1993 Direction numerical simulations of turbulent flow over a backward-facing step. *Proc. 9th Symp. on Turbulent Shear Flows.* **2,** 13.2.1-13.2.5.

LIEN, F. S. AND LESCHZINER, M. A. 1993 A pressure-velocity solution strategy for compressible flow and its application to shock/boundary-layer interaction using second-moment turbulence closure. *ASME J. Fluids Engineering.* **115,** 717-725.

LIEN, F. S. AND LESCHZINER, M. A. 1994a A general non-orthogonal collocated finite volume algorithm for turbulent flow at all speeds incorporating second-moment closure, Part 1: Computational implementation, Part 2: Application. *Comput. Methods Appl. Mech. Eng.* **114,** 123-167.

LIEN, F. S. AND LESCHZINER, M. A. 1994b Upstream monotonic interpolation for scalar transport with application to complex turbulent flows. *Int. J. Numer. Methods Fluids.* **19,** 527-548.

LIEN, F. S. & LESCHZINER, M. A. 1995a Modeling 2D separation from a high-lift aerofoil with a non-linear eddy-viscosity model and second-moment closure. *Aeronautical J.* **99,** 125-144.

LIEN, F.S. & LESCHZINER, M.A. 1995b Computational modeling of multiple vortical separation from streamlined body at high incidence. *Proc. 10th Symp. on Turbulent Shear Flows.* **1,** 4.19-4.24.

LIEN, F. S., CHEN, W. L. & LESCHZINER, M. A. 1996 Low-Reynolds-number eddy-viscosity modeling based on non-linear stress-strain/vorticity relations. *Engineering Turbulence Modeling and Experiments.* **3,** W. Rodi & G Bergeles (ed.) 91-101.

KIM, J., MOIN, P. & MOSER, R. D. 1987 Turbulence statistics in fully-developed channel flow at low Reynolds number. *J. Fluid Mech.* **177,** 133-166.

POPE, S. B. 1975 A more general effective-viscosity hypothesis. *J. Fluid Mech.* **72,** 33-340.

RHIE, C. M. & CHOW, W. L. 1983 Numerical study of the turbulent flow past an airfoil with trailing edge separation. *AIAA J.* **21,** 1525-1532.

ROGERS, S. E. & KWAK, D. 1990 Upwind differencing scheme for the time-accurate incompressible Navier-Stokes equations. *AIAA J.* **28,** 253-262.

SPEZIALE, C. G. 1987 On non-linear $K - l$ and $k - \varepsilon$ models of turbulence. *J. Fluid Mech.* **178,** 459-475.

SPALART, P. R. 1988 Direction simulation of a turbulent boundary layer up to $R_\theta = 1410$. *J. Fluid Mech.* **187,** 61-98.